UTRECHT UNIVERSITY

MASTER THESIS

MR methods for imaging of acoustic radiation force in tissue

October 28, 2010

Author:
Elma CARVAJAL GALLARDO BSc
Graduate School of Life Sciences
Faculty of Science

Supervisor:
Dr. L.W. BARTELS
Associate Professor
MR Physics Group
Image Sciences Institute
University Medical Center Utrecht

Abstract

In this thesis the theory behind acoustic radiation force and the theory of elasticity are presented, which are used to characterize tissue displacements due to (acoustic) radiation force. The beginning of the development of ultrasound elastography is discussed, which forms the basis of the development of MR methods to image tissue displacement due to acoustic radiation force. These MR methods will be discussed and literature concerning the comparison to ultrasound methods and clinical applications is reviewed.

Contents

1 Introduction & outline

Changes in tissue elasticity are generally correlated with pathological phenomena, such as cancers and cysts [1]. In clinical practice the changes in tissue elasticity are usually detected by manual palpation. However, manual palpation is not quantitative, and tissues deep in the body cannot be reached [2].
Therefore imaging methods have been developed which can be used to quantify tissue elasticity. One of the first methods to quantify tissue elasticity is called elastography and uses ultrasound to detect tissue displacement caused by external compression of the tissue ([1],[3]). As will be shown, this displacement can be related to tissue elasticity, thus allowing the quantifying of tissue elasticity. However, imaging deep into tissue still forms an obstacle with these methods, in addition to the problems caused tissues which are invisible to ultrasound.
To be able to image deep into tissue, MR methods have been developed to image deep in to tissue. Some of these MR methods use external excitation of the tissue, while other methods use (focused) ultrasound in order to create displacements.
The displacements created by (focused) ultrasound are caused by a general mechanism called (acoustic) radiation force, which comprises a unidirectional force, causing displacement of (elastic) tissue, due to the transfer of momentum.
In this thesis we will introduce the physical theory behind this (acoustic) radiation force and we will treat the theory of elasticity in order to characterize tissues. After having laid a theoretical foundation we will discuss the beginning of elastography, and the development of MR methods for imaging displacement caused by acoustic radiation force in tissue, such as MR elastography (MRE) and MR acoustic radiation force imaging (MR-ARFI). Furthermore we will discuss recent research which implies that MR methods for imaging acoustic radiation force in tissue show promising results for using these methods in clinical applications, for example in the staging of liver fibrosis, the diagnosis of breast lesions and US transcranial therapy.

2 Acoustic radiation force

2.1 General theory

Acoustic radiation force, also called acoustic radiation pressure in literature [4], describes the universal phenomenon that a unidirectional force is exerted on the surface of an object when finite-rest-energy of zero-rest-energy particles are absorbed or reflected by that surface ([5],[6]). The term acoustic radiation pressure is somewhat unfortunate, while pressure usually refers to a scalar quantity, as opposed to the vector quantity representing acoustic radiation force [4].
In this section we will derive the acoustic radiation force following the approach of Landau and Lifshitz [7] in their treatment of the momentum flux.

For ideal fluids the equation of continuity is given by [7]:

$$\frac{\partial \rho}{\partial t} + \nabla \cdot (\rho \vec{v}) = 0, \tag{1}$$

or equivalently in tensor notation,

$$\frac{\partial \rho}{\partial t} = -\frac{\partial (\rho v_k)}{\partial x_k}, \tag{2}$$

where $\rho = \rho(x, y, z, t)$ is the fluid density and $\vec{v} = \vec{v}(x, y, z, t)$ represents the distribution of fluid velocity, both of which are functions of the coordinates x, y and z and the time t.
The equation of motion of the ideal fluid, neglecting gravitational terms, is called Euler's equation and is given by [7]:

$$\frac{\partial \vec{v}}{\partial t} + (\vec{v} \cdot \nabla)\vec{v} = -\frac{1}{\rho}\nabla p, \tag{3}$$

or again in tensor notation,

$$\frac{\partial v_i}{\partial t} = -v_k \frac{\partial v_i}{\partial x_k} - \frac{1}{\rho}\frac{\partial p}{\partial x_i}, \tag{4}$$

where $p = p(x, y, z, t)$ represents the pressure.
As has been demonstrated by Landau and Lifshitz [7] the equation of continuity (2) and Euler's equation (4) can be combined to obtain:

$$\frac{\partial}{\partial t}(\rho v_i) = -\frac{\partial \Pi_{ik}}{\partial x_k}, \tag{5}$$

where Π_{ik} is a symmetrical tensor of rank two, defined as:

$$\Pi_{ik} = p\delta_{ik} + \rho v_i v_k. \tag{6}$$

By integrating equation (5) over some volume V and by using the divergence theorem, we find [7]:

$$\frac{\partial}{\partial t}\int_V (\rho v_i) dV = -\oint_{\partial V} \Pi_{ik} n_k df, \tag{7}$$

where n_k is the kth component of the unit vector $\hat{n}$ along the outward normal, dV is the area of the volume element and df is the area of the surface element.
In equation (7) the left-hand side is the time derivative of the ith component of the momentum of the volume V. Necessarily, the right-hand side must be the amount of momentum flowing out through the bounding surface ∂V in unit time [7]. The tensor Π_{ik} is called the momentum flux density tensor.
The theory presented above, as developed by Landau and Lifshitz [7], can be written in vector notation, when representing the momentum flux density tensor Π_{ik} in matrix notation as $\mathbf{\Pi}$. Using this notation, we find for equation (5):

$$\frac{\partial}{\partial t}(\rho \vec{v}) = -\nabla \cdot \mathbf{\Pi}. \tag{8}$$

Using equation (6) we find:

$$\mathbf{\Pi} \cdot \hat{n} = p\hat{n} + \rho\vec{v}(\vec{v} \cdot \hat{n}). \tag{9}$$

We can average equation (8) to find:

$$\overline{\nabla \cdot \mathbf{\Pi}} = \vec{0}, \tag{10}$$

where the overline is used to indicate time averaging,

$$\overline{f} \equiv \lim_{T\to\infty} \frac{1}{2T}\int_T^T f(t)dt. \tag{11}$$

If the function $f(t)$ remains bounded, it can be seen that the time average of $\frac{\partial f}{\partial t}$ must vanish [4]. This has been used to obtain equation (10), while $\rho\vec{v}$ is a physical function, and thus remains bounded.
Equation (10) can be integrated over some volume V to find:

$$\int_V \overline{\nabla \cdot \mathbf{\Pi}} dV = \oint_{\partial V} \overline{\mathbf{\Pi} \cdot \hat{n}} df = \vec{R}, \tag{12}$$

where the divergence theorem has been used, and where $\vec{R}$ represents a constant vector.
Equivalently, using equation (9):

$$\oint_{\partial V} \left(\overline{p}\hat{n} + \overline{\rho\vec{v}(\vec{v} \cdot \hat{n})}\right) df = \vec{R}. \tag{13}$$

We define averaging over any region U fixed in space as:

$$\langle f \rangle \equiv \frac{\int_U f dU}{\int_U dU}. \tag{14}$$

Using this in equation (13) gives:

$$\oint_{\partial V} \left(\langle \overline{p} \hat{n} \rangle + \langle \overline{\rho \vec{v} (\vec{v} \cdot \hat{n})} \rangle \right) df = \vec{R}. \tag{15}$$

In deriving equation (15) above, the claim made by Livett et al. [4] in section 2.1 that his treatment can be extended to three dimensions, has been verified. It should be noted however, that the constant vector $\vec{R}$ in equation (15) has different dimensions than the constant R used by Livett et al. [4] in section 2.1. In fact, to obtain the exact analogue of the constant R in Livett et al. [4], equation (15) should be divided by $\oint_{\partial V} df$.
According to Livett et al. [4] the constant R characterizes the field as a fundamental property of the acoustic field. They suggest that the quantity $R - p_0$ be called the radiation pressure, where p_0 is the hydrostatic pressure in the absence of the acoustic field. Analogously, we may conclude that the constant vector $\vec{R}$ found in equation (15) is a fundamental property of the three dimensional acoustic field. Furthermore we see that the vector $\frac{\vec{R}}{\oint_{\partial V} df} - \vec{p_0}$ can be called the radiation pressure, where $\vec{p_0}$ is a constant vector. Equivalently, $\vec{R} - \vec{p_0} \oint_{\partial V} df$ may be called the radiation force, or by using equation (15):

$$\vec{F} = \oint_{\partial V} \left(\langle \overline{p} \hat{n} \rangle - \vec{p_0} + \langle \overline{\rho \vec{v} (\vec{v} \cdot \hat{n})} \rangle \right) df, \tag{16}$$

where $\vec{F}$ represents the radiation force.
Equivalently, the radiation force may also be expressed in a slightly different way by using equation (13):

$$\vec{F} = \oint_{\partial V} \left(\overline{p} \hat{n} - \vec{p_0} + \overline{\rho \vec{v} (\vec{v} \cdot \hat{n})} \right) df, \tag{17}$$

Another, more physical derivation of the acoustic radiation force has been done by Torr [6]. In his treatment of the radiation force, Torr uses Euler's momentum theorem for ideal fluids, an analogue of Newton's second law of motion, which states that the resultant of body forces acting on an enclosed fluid is equal to the rate of change of momentum plus the rate of flow of momentum outwards through the bounding surface [6].
Comparing the radiation force found in equation (17) to the radiation force found by Torr [6], we see that these two are equal, when we keep in mind that Torr already has subtracted the constant hydrostatic pressure from the pressure term.
Furthermore, in his derivation of the radiation force, in section II Torr gives a physical explanation why the average rate of change of momentum must be equal to zero, complementary to the justification which led to equation (10).

2.2 Interpretation

In their work Livett et al. [4] provide some calculations supporting their claim that the quantity $R - p_0$ be called the radiation pressure. In the case of a rigid target, they use the fact that the velocity at the surface of the target must equal zero, to show that $R = (\overline{p})_{surface}$. They conclude that this is experienced by the target as a force, and thus may be associated with radiation pressure. Analogously, in our three dimensional case, we find that for a rigid target the radiation force is equal to $\vec{F} = \oint_{\partial V} (\overline{p} \hat{n} - \vec{p_0}) df$, exactly as one would expect.
After having treated the case of a rigid target in section 2.2, Livett et al. [4] treat the case of a non-rigid target in section 2.3 to further support their claim of associating the $R - p_0$ with the radiation pressure. In their argument, they use Lagrangian coordinates, with a frame of reference centered around the fluid elements, i.e. the coordinates are not fixed in space, but fixed in the fluid elements. This is in contrast to Eulerian coordinates, which are fixed in space.

In their argument Livett et al. [4] start with the one dimensional equation of motion in Lagrangian coordinates, as has been derived by Beyer in his book on nonlinear acoustics [8]:

$$-\frac{\partial p_L}{\partial x} = \rho_0 \frac{\partial^2 \xi}{\partial t^2}, \tag{18}$$

where the subscript L refers to the Lagrangian coordinates used, ξ represents the particle displacement and ρ_0 is the constant fluid density in absence of the field.
Using equation (18) Livett et al. [4] then argue that $\overline{p_L}$ must be constant, by integrating the averaged equation (18), suggesting that $\overline{p_L}$ and R must be related. Livett et al. use a mathematical proof to support their claim. However, they seem to have made a mistake in their proof, which fortunately does not compromise the validity of their claim. A modified proof, following the proof of Livett et al. in section 2.3 [4] can be found in the appendix A.
Using this proof, the constant R is equal to the Lagrangian average pressure. Thus justifying the name radiation pressure for the constant R, as Livett et al. conclude.

2.3 Relating radiation force to beam power

In literature, radiation power is usually associated with energy density or intensity, while these are useful quantities in ultrasound measurements ([4],[6],[9],[10],[11]).
An elegant derivation relating radiation force to beam power can be found in the work of Joyce [5]. Here Joyce uses an argument based on adiabatic invariance to show that the radiation force on a reflecting object is equal to:

$$|\vec{F}| = \frac{W}{c}, \tag{19}$$

where W represents the bilateral beam power and c the phase velocity.
An alternative derivation has been presented by Torr [6]. Torr argues that a mean sound pressure in the beam that differs from the sound pressure elsewhere in the medium, would lead to movement of liquid either out of or into the beam, thus equalizing the mean sound pressure in the medium. The effect would be to decrease or increase the mean sound pressure $\overline{p}$ to $\vec{p_0}$, reducing equation (17) to:

$$\vec{F} = \oint_{\partial V} \overline{\rho \vec{v}(\vec{v} \cdot \hat{n})} df. \tag{20}$$

Using the fact that the mean kinetic energy density equals $\frac{\rho v^2}{2}$ and the (simplified) fact that the mean potential energy density equals the mean kinetic energy density, we can then conclude, analogous to Torr [6], that:

$$|\vec{F}| = \oint_{\partial V} \overline{\rho |\vec{v}|^2 \cos\theta} df = \oint_{\partial V} \overline{E} df, \tag{21}$$

where θ is the angle between the velocity $\vec{v}$ and the normal vector $\hat{n}$ and $\overline{E}$ is the total mean energy density.
Finally, as Torr argues [6], the total mean energy density $\overline{E}$ is related to the ultrasonic beam power W by $\overline{E} = \frac{W}{c \oint_{\partial V} df}$, so that:

$$|\vec{F}| = \frac{W}{c}, \tag{22}$$

for an absorbing target.
Even though equation (19) and (22) look identical, a distinction should be made. While the former represents the radiation force on a reflecting target, the latter represents the radiation force on an absorbing target. Thus, the bilateral beam power W in the former is twice the beam power W in the latter.
Unfortunately the result obtained above in equation (22) has been proven valid only in the special case of dealing with a medium of constant compressibility ([6],[4]). However, we will not derive the results for different cases here, while the literature considered in this thesis uses equation (22) as a basis.

The theory describing acoustic radiation force derived in the previous sections only described radiation force due to plane ultrasonic waves traveling in ideal fluids. Acoustic radiation force has also been derived for focused ultrasound (FUS) ([12],[13],[14],[15]), but as the tracing of some key references describing the mathematical background on which the authors base their theories has proven very difficult, the treatment of these papers will be left out of this thesis. Consequently we will work with the idealized acoustic radiation force, while most of the literature presently known uses this treatment of acoustic radiation force, or even only uses the fact that acoustic radiation force can displace tissue, without using any assumptions relating this radiation force to other measurable quantities.

3 Theory of elasticity

In the last chapter we considered the acoustic radiation force. Now we will turn to the theory of elasticity, while biological tissues usually exhibit elastic behavior. In the previous section acoustic radiation force has been treated for ideal fluids only. Even though human tissue cannot be considered an ideal fluid, the treatment of acoustic radiation force in the previous chapter shows that a force will be exerted onto the tissue when applying ultrasound to it. This force will eventually be balanced by the elastic force in the tissue itself, resulting in a steady state displacement, instead of flow, as would be expected in a fluid.

3.1 General theory

We treat the theory of elasticity for isotropic bodies by following the book of Landau and Liftshitz [16].

When forces are applied to solid bodies, they exhibit a deformation to some extent, which means that their shape and volume changes. We can consider a particular point in such a solid body. Let the radius vector before deformation be $\vec{r}$ and after deformation $\vec{r'}$. Then the displacement of this point due to this deformation can be represented by the displacement vector $\vec{u}$, as a function of the coordinates x_i of the radius vectors: $u_i = x'_i - x_i$. Now consider two points close together. The distance between these points changes due to the deformation. Let dl be the distance between the points before deformation and dl' after deformation. Landau and Lifshitz [16] show that these two quantities are related in the following way:

$$dl'^2 = dl^2 + 2u_{ik}dx_i dx_k, \tag{23}$$

with:

$$u_{ik} = \frac{1}{2}\left(\frac{\partial u_i}{\partial x_k} + \frac{\partial u_k}{\partial x_i} + \frac{\partial u_l}{\partial x_i}\frac{\partial u_l}{\partial x_k}\right). \tag{24}$$

The tensor u_{ik}, which is symmetrical, is called the strain tensor.
As discussed by Landau and Lifshitz [16], for small deformations, second order terms are neglected:

$$u_{ik} = \frac{1}{2}\left(\frac{\partial u_i}{\partial x_k} + \frac{\partial u_k}{\partial x_i}\right). \tag{25}$$

The equations above describe three dimensional situations. However, when we consider the one dimensional analogue, the equations simplify considerably. The one dimensional strain is given by:

$$strain = \frac{\partial u}{\partial x}. \tag{26}$$

As described by Landau and Lifshitz [16], when a body is deformed forces will occur which tend to return the body to equilibrium. These forces are called internal stresses.
Let the force per unit volume of a body due to internal stresses be represented by the vector $\vec{F}$. Then the components of this force are given by [16]:

$$F_i = \frac{\partial \sigma_{ik}}{\partial x_k}, \tag{27}$$

where the tensor σ_{ik} is called the stress tensor.
In case of an arbitrary deformation σ_{ik} can have off-diagonal non-zero elements, which lead to shearing (tangential) stresses on each surface element. These shearing stresses are the driving force behind the movement of surface elements relative to each other [16].
Now the total force on the body due to internal stresses can be calculated by:

$$\int_V F_i dV = \oint_{\partial V} \sigma_{ik} n_k df. \tag{28}$$

Deformations of bodies can be divided into two separate groups [16]. The first group is the group of elastic deformations. Elastic deformations are characterized by the return of the body to its original undeformed state when the forces causing the deformation cease to act, given that the deformation of the body is small. The second group is the group of plastic deformations. In this case residual deformation remains when the forces causing the deformation cease to act. The theory of elasticity focuses on this first group of deformations. And because acoustic radiation force used in medical applications only has the goal of causing elastic deformations in tissues, we will only consider elastic deformations in what follows.

As Landau and Lifshitz [16] have derived, the free energy can be related to the stress tensor as follows:

$$dF = -SdT + \sigma_{ik} du_{ik}, \tag{29}$$

where F is the free energy, S is the entropy and T is the temperature.
Now, the stress tensor can be found from the free energy by using the following identity:

$$\sigma_{ik} = \left(\frac{\partial F}{\partial u_{ik}} \right)_T, \tag{30}$$

where the subscript T refers to taking the derivative while keeping the temperature constant.
As Landau and Lifshitz [16] argue, when expanding the free energy in powers of u_{ik}, terms of first order can be neglected. Therefore the second order expansion of the free energy takes the form:

$$F = F_0 + \frac{1}{2}\lambda u_{ii}^2 + \mu u_{ik}^2, \tag{31}$$

where λ and μ are called the Lamé coefficients.
Alternatively, the free energy can also be written as [16]:

$$F = \mu(u_{ik} - \frac{1}{3}\delta_{ik} u_{ll})^2 + \frac{1}{2} K u_{ll}, \tag{32}$$

with:

$$k = \lambda + \frac{2}{3}\mu, \tag{33}$$

where the Lamé coefficient μ is called the shear modulus and K is called the bulk modulus. Both of these moduli are strictly positive.
In obtaining equation (32) the following identity has been used [16]:

$$u_{ik} = (u_{ik} - \frac{1}{3}\delta_{ik} u_{ll}) + \frac{1}{3}\delta_{ik} u_{ll}. \tag{34}$$

In this identity the first term represents pure shear, which does not change the volume of the body, but only changes its shape. The second term represents hydrostatic pressure, which has the opposite effect of only

changing the volume of the body but not its shape. Accordingly, μ is also called the modulus of rigidity and K the modulus of hydrostatic compression.

We now look at homogeneous deformations, where the strain tensor is considered constant throughout the whole volume of the body, and consider the case of the simple compression of a rod. The component u_{zz} gives the relative lengthening of the rod in terms of the coefficient of extension $p = \sigma_{zz}$ and the modulus of extension or Young's modulus E [16]:

$$u_{zz} = \frac{\sigma_{zz}}{E} = \frac{p}{E}, \tag{35}$$

where:

$$E = \frac{9K\mu}{3K + \mu}. \tag{36}$$

The ratio of the transverse compression to the longitudinal extension is called Poisson's ratio σ [16]:

$$u_{xx} = -\sigma u_{zz}, \tag{37}$$

where:

$$\sigma = \frac{1}{2}\frac{3K - 2\mu}{3K + \mu}. \tag{38}$$

A general formula relating the stress tensor to the strain tensor in terms of the Young modulus and Poisson's ratio is given by [16]:

$$\sigma_{ik} = \frac{E}{1+\sigma}\left(u_{ik} + \frac{\sigma}{1-2\sigma}u_{ll}\delta_{ik}\right). \tag{39}$$

We should note however, that the second order approximation of the free energy has been used to obtain this equation.

3.2 Elastic Waves

Now that the general theory has been derived above, we consider elastic waves, again following Landau and Lifshitz [16]. We make the assumption that the motion is adiabatic, i.e. no heat exchange occurs between different parts of the body under consideration. In an adiabatic transformation the stress tensor σ_{ik} is given in terms of the strain tensor u_{ik} by the usual formulae, but the values of E and σ need to be replaced by their adiabatic values [16].

We start with the general equation of motion, by using equation (27):

$$\rho\ddot{u}_i = \frac{\partial \sigma_{ik}}{\partial x_k} \tag{40}$$

Now substitute equation (39) and (25) into equation (40) to obtain [16]:

$$\rho\ddot{\vec{u}} = \frac{E}{2(1+\sigma)}\triangle\vec{u} + \frac{E}{2(1+\sigma)(1-2\sigma)}\nabla(\nabla\cdot\vec{u}), \tag{41}$$

where ρ is the density of the body.
Note that the first order approximation of the strain tensor has been used to arrive at this equation.

We can consider the deformation $\vec{u}$ to consist of three different parts: a longitudinal part $\vec{u}_l$, a transverse part $\vec{u}_t$ and a harmonic part $\vec{u}_h$, i.e. $\vec{u} = \vec{u}_l + \vec{u}_t + \vec{u}_h$, which obey the following conditions [16]:

$$\nabla \times \vec{u}_l = 0, \tag{42}$$
$$\nabla \cdot \vec{u}_t = 0, \tag{43}$$
$$\nabla \times \vec{u}_h = 0, \tag{44}$$
$$\nabla \cdot \vec{u}_h = 0. \tag{45}$$

Now using the vector identity $\nabla(\nabla \cdot \vec{u}) = \triangle \vec{u} + \nabla \times \nabla \times \vec{u}$ we find:

$$\rho \ddot{\vec{u}} = \frac{E(1-\sigma)}{(1+\sigma)(1-2\sigma)} \nabla(\nabla \cdot \vec{u}) - \frac{E}{2(1+\sigma)} \nabla \times \nabla \times \vec{u} \tag{46}$$
$$= (\lambda + 2\mu)\nabla(\nabla \cdot \vec{u}) - \mu(\nabla \times \nabla \times \vec{u}). \tag{47}$$

We can now take the curl of equation (47) above to obtain the (linear) shear wave equation:

$$\rho \frac{\partial^2}{\partial t^2}(\nabla \times \vec{u}) = \mu \nabla^2 (\nabla \times \vec{u}), \tag{48}$$

or equivalently:

$$\rho \frac{\partial^2}{\partial t^2}(\nabla \times \vec{u_t}) = \mu \nabla^2 (\nabla \times \vec{u_t}), \tag{49}$$

where the velocity of propagation β_t is given by:

$$\beta_t^2 = \frac{\mu}{\rho}. \tag{50}$$

By taking the divergence of equation (47) we find the (linear) longitudinal wave equation:

$$\rho \frac{\partial^2}{\partial t^2}(\nabla \cdot \vec{u}) = (\lambda + 2\mu)\nabla^2 (\nabla \cdot \vec{u}), \tag{51}$$

or equivalently:

$$\rho \frac{\partial^2}{\partial t^2}(\nabla \cdot \vec{u_l}) = (\lambda + 2\mu)\nabla^2 (\nabla \cdot \vec{u_l}), \tag{52}$$

where the velocity of propagation β_l is given by:

$$\beta_l^2 = \frac{\lambda + 2\mu}{\rho}. \tag{53}$$

It should be noted that in de derivation of these wave equations above, the linear strain tensor in equation (25) has been used. Thus, we derived the linear shear and longitudinal wave equations. The non-linear wave equations can also be derived, by using the general strain tensor in equation (24). However, we will not derive those wave equations here.

Little can be found in literature concerning acoustic radiation force in elastic tissues. Therefore we will not treat this subject in this thesis, and will now consider the applications of the theories derived above in literature.

4 Elastography

In this section we discuss two papers, which mark the beginning of elastography. The first paper is from Ophir et al. [1] and the second paper is from Céspedes et al. [3]. In the former, the basis of elastography is discussed, showing that elastography using external mechanical compression can be used to measure elastic properties of tissue. In the latter a linear array transducer is used as an ultrasound scanner and the elastograms are measured in vivo. Both of the papers describe methods using ultrasound to measure the displacements by making use of correlation techniques.

Changes in tissue elasticity are generally related with pathological phenomena, such as cancers or fluid filled cysts. Usually these pathological lesions are located deep in the body or have a very small size, making its detection by palpation difficult. Furthermore, the absence of echogenic properties of the lesion may make it invisible for ultrasonic detection [1].
Therefore, Ophir et al. propose a new method for strain and Young modulus imaging of soft tissues, which is a better alternative for previously developed methods, because of its ability to provide more quantitative information [1]. The goal of their method is to produce two dimensional images, called elastograms, in which the inverse Young modulus is displayed.
The first step in obtaining an elastogram is called strain profiling [1], in which an external axial compression stimulus is applied to tissue to produce strain. This strain is imaged in a plot called a strain profile as a function of depth, by using equation (26). After that a two dimensional strain image is formed by joining many of such strain profiles.
Because strain is for example dependent on initial compression [1], its quantitative value is limited. Therefore Ophir et al. propose to convert the strain profile to a Young modulus or elastic modulus profile. The authors argue that, since the stress remains constant with depth in a one dimensional model, by applying a known stress to the tissue, the strain profiles can be converted to Young modulus profiles by using equation (35). Ophir et al. propose to measure the applied stress by using an anterior compliant standoff layer with a known Young modulus. And again by using equation (35) the applied stress on this layer can then be calculated from the strain profile.
The last step in obtaining an elastogram now consists of inverting the Young modulus image.

In obtaining the strain profiles, two A-line measurements are compared, one before compression of the tissue and one after compression, obtained from a total depth of 12 cm which has been broken up into segments. Ophir et al. propose to use the temporal location of the maximum peak of the cross-correlation function of these two measurements as the time shift between the data in two corresponding segments under consideration [1]. In this way the time shift is calculated between all corresponding segments in the A-lines. The corresponding strain profile is then defined by using equation (26):

$$s_i = \frac{\triangle l}{l} = \frac{\triangle t}{t} = \frac{t_{i+1} - t_i}{2\frac{dz}{c}}, \tag{54}$$

where s_i is the strain for the ith segment pair, $\triangle l$ is the difference in length between the ith pair segments, l is the total difference in length between the A-lines, $\triangle t$ is the difference in time between the ith pair segments, t is the time, t_{i+1} and t_i are the (i+1)th and ith time shifts, dz is the length of a segment and c is the speed of sound in the tissue [1].
It should be noted that Ophir et al. assume simple linear motion in the tissue at constant velocity to obtain this formula. Also, they assume that the speed of sound in the tissue is constant before and after the compression. However, this is not necessarily correct, as has been shown by Walker [11]. Unfortunately, Ophir et al. do not mention this in their paper.

In constricting the three dimensional strain to one dimension, the actual stress throughout the volume is overestimated. The reason for this is that shearing stresses, which play a role in realistic three dimensional situations are overlooked. As has been derived by Saada, a more realistic axial stress function is given by [17]:

$$\sigma_{zz} = q\left(-1 + \frac{z^3}{(a^2+z^2)^{\frac{3}{2}}}\right), \tag{55}$$

where a pressure distributed uniformly over a circular area is considered, known as the Boussineq problem. In the formula above q represents the uniformly distributed pressure, a represents the radius of the circular area and z represents the depth in the elastic medium.
As can be seen from equation (55) above, the axial stress is now a function of depth, and not necessarily constant. Ophir et al. recognize this problem and discuss the findings of Saada in the appendix of their work [1]. However, they argue that for $\frac{z}{a} \leq 1$ there is only a small reduction in axial stress and thus they conclude that by using a large area of compression, the one dimensional approach can be justified.
One of the experiments performed by Ophir et al. is to compare the theoretical predictions for the axial stress as in equation (55) to the experimentally calculated axial stress. As Ophir et al. explain, they use the strain data which they assume proportional to the axial stress, since they are not able to make direct stress measurements. However, as can be found in Landau and Lifshitz [16] this is not generally true, because in reality the experiments are done in three dimensions, making equation (35) invalid in this case. Instead, equation (39) gives a more realistic view of the situation, and shows a more complex dependence of the stress tensor elements on the strain tensor elements.
In addition, Ophir et al. conclude that it is clear from their experiments *that the general behavior of the strain follows the theoretical predictions reasonably well*. However, the authors do not support their claim in any way. Moreover the validity of their claim may be doubted.
Also, the standard deviation in the Young modulus measurements is rather high [1]. A reason for this may be the use of boundary conditions (estimating the applied stress) when calculating the Young modulus.
However, overall the results presented by Ophir et al. do show that their technique has the potential of quantitatively imaging the inverse elastic modulus in soft tissues [1].

The technique presented by Ophir et al. [3] has been further developed by Céspedes et al. by using an ultrasound scanner equipped with a linear array transducer. In addition, Céspedes et al. also present elastograms which have been obtained in vivo, for which the system used by Ophir et al. was not suitable [3].
Céspedes et al. use the same approach as Ophir et al. in obtaining their elastograms and the authors still assume a constant axial stress. However, in contrast to Ophir et al., Céspedes et al. do mention the assumption of a constant speed of sound in obtaining equation (54).
The in vivo experiments done by Céspedes et al. are performed in the right leg of a male volunteer and in breast studies of healthy volunteers and one breast cancer patient. To minimize sources of motion, a mammography compression paddle is used to hold the tissue in position and in the breast studies the human volunteers are asked to hold their breath during the scan time [3].
Especially noteworthy in the results of the experiments performed by Céspedes et al. is the appearance of the cancer nodule as a well delineated black area in the elastogram of the breast cancer patient. The lesion is better visible in the elastogram than in the sonogram: in the sonogram, the lesion appears to have a relatively strong shadow, which makes the shape and size of the lesion hard to determine in the sonogram [3].

In conclusion, the results shown by by Céspedes et al. [3] indicate that elastography can provide quantitative information about the elasticity of tissues, in vivo. This is supported by Plewes et al. [2], which we will consider below. However, by making use of external mechanical compression, tissues deep in the body remain hard to reach.
Unfortunately, the one dimensional approach used by Ophir et al. [1] and by Céspedes et al. [3] limits the general applicability of the method. In contrast, the possibility to use volumetric acquisitions in MRI facilitates the estimation of all strain components, as will be shown later ([18],[19]). This is a unique advantage of MRI over ultrasound based methods. Consequently, the method developed by Ophir et al. [1] and Céspedes et al. [3] has been further developed to include three dimensional imaging of tissue displacement with MRI.

5 Imaging of external compression with MRI

One of the next steps towards imaging acoustic radiation force with MRI is done by Plewes et al. [2]. Still, displacements in tissues are obtained by external compression, but this time, in contrast to the previous papers ([1],[3]), MRI is used to visualize this displacement, thus showing that elastography can be done by using MRI. Plewes et al. propose to use transient mechanical compression of tissue in combination with a phase contrast MR sequence, using a spin-echo pulse sequence and motion-sensitizing gradient pulses. In figure 1 the MR sequence has been displayed.

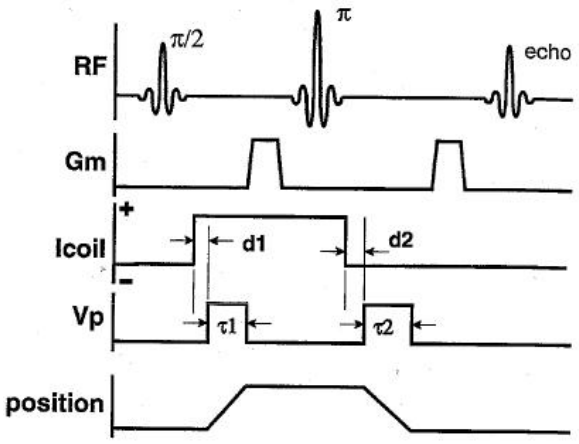

Figure 1: Motion-sensitized MR sequence diagram. RF waveforms (top) with motion-sensitizing gradients (G_m), the current applied to the coil driving the compression plate (I_{coil}) and the transit time voltage (V_p). Source: Plewes et al. [2]

As has been derived by Haacke et al. the accumulated phase $\phi_v(\vec{r})$ due to the motion-sensitizing gradients, which have been displayed in figure 1, is described by [20]:

$$\triangle\phi_v(\vec{r}) = 2\gamma G v(\vec{r})\tau^2 = 2\gamma G x(\vec{r})\tau, \tag{56}$$

where γ is the gyromagnetic ratio, G is the gradient strength, $v(\vec{r})$ is the velocity of the spins, τ is the duration of the gradient and $x(\vec{r})$ is the displacement. Here the assumption has been made that the motion-sensitizing gradients are rectangular and simple linear motion has been assumed.
The method used by Plewes et al. is to first image a phantom using the sequence displayed in figure 1. The phase of the resulting spin-echo image is then subtracted from a spin-echo image using the same sequence, while no compression is applied. The resulting phase images are then unwrapped and converted into displacement images using equation (56) [2].
The advantage of using MRI for calculating the displacement by use of motion-sensitizing gradients is that the motion in any arbitrary direction can be measured, simply by adjusting the (combination of) gradients which are being used. Plewes et al. use this to measure separate component displacement images which have been formed while adjusting the orientation of the motion-sensitizing gradients through three orthogonal directions. These component displacement images are then combined to form a magnitude image. Finally, a strain image can be calculated as the gradient of the magnitude image following equation (26) [2].
The experiments done by Plewes et al. use two phantoms consisting of various gel materials which simulate spatially varying tissue compliance. The Young modulus is calculated for each gel material analogously to the methods used by Ophir et al. [1] and Céspedes et al. [3], again implying that boundary conditions are used. Following this methods, first the compression resulting from a known uniaxial loading of a 1 cm^3 sample of each gel material is measured [2], after which the Young modulus is obtained by using equation (35).

The results of the experiments performed on the phantoms show that shear displacement can be seen more clearly than longitudinal displacement. The authors observe that the presence of different gel layers within the phantoms is not clear from the longitudinal scans. Instead, the shear displacement images show a better differentiation between the different layers. Moreover, complex patterns are seen in the shear displacement images. Plewes et al. conclude that the data show the need for detecting all three components of motion to clearly differentiate between the different gel layers [2].
An explanation for the absence of differentiation between the different gel layers in the longitudinal images may be that the longitudinal displacement decreases rapidly with distance. The compression plate used has a diameter of 6 cm while the image depth is equal to 12 cm. Following the reasoning of Ophir et al. [1] and using equation (55) $\frac{z}{a} = 4 > 1$, which may explain these results. Clearly, the use of equation (35) cannot be justified here anymore.
This problem of rapidly decreasing longitudinal displacement has been overcome by considering solely shear displacements and working with the shear modulus instead of the Young modulus in characterizing tissue compliance, thereby setting the next step towards imaging acoustic radiation force with MRI.

6 Magnetic resonance elastography

Just shortly after Plewes et al. [2] was published, a paper from Muthupillai et al. [19] was published in which the external compression used in Plewes et al. to generate displacement in tissue is replaced by harmonic mechanical excitation of the tissue, resulting in propagating acoustic strain waves in the tissue. In the method developed by Muthupillai et al. [19] called magnetic resonance elastography (MRE), not only displacement of the tissue is visualized, but from that information, the shear modulus of the tissue is imaged, in contrast to the Young modulus used in the previous papers ([1],[2],[3]).
Muthupillai et al. propose to use harmonic mechanical excitation to create harmonic displacements in tissue, where the direction of vibration of the electromechanical actuator is orthogonal to the normal vector to the surface. In this way, not only longitudinal, but also shear waves are created in the tissue [19].
Even though MRE uses harmonic mechanical excitation, instead of an ultrasound transducer, to couple the acoustic waves into the tissue, MRE as described by Muthupillai et al. ([18],[19]) can be regarded as the forerunner of imaging acoustic radiation force with MRI, when realizing that the simplest ultrasound transducer is nothing more than a vibrating piezo element, used to couple acoustic waves into tissue. It is true that the frequencies used by Muthupillai et al. ([18],[19]) are much lower that the frequencies used in medical ultrasound. However, the theory behind acoustic radiation force does not make any conditions regarding the frequency of the acoustic waves ([4],[5],[6],[7]).
An intuitive justification of the fact described above can also be given. When using a low frequency acoustic waves, the tissue will be displaced back and forth at the frequency of the acoustic waves. When the frequency of the waves increases the tissue will not have time to relax after a 'push' of sound pressure, due to viscosity of the tissue, and thus the tissue will eventually displace only in one direction, in the direction of propagation of the acoustic waves.
The situation described by Muthupillai et al. ([18],[19]) corresponds to the first situation described above. And even though shear waves are imaged with this method, still acoustic radiation force is used, be it in the form of acoustic shear waves, instead of longitudinal (compressional) waves.
As we will see later, for example as described by Wu et al. [21], MRE as described by Muthupillai et al. ([18],[19]), has been developed further to image the (shear) displacements, generated by FUS, which corresponds to the high frequency case as described above.

6.1 Magnetic resonance elastography with mechanical strain waves

MRE is a method developed by Muthupillai et al. to image and quantitate displacements generated by harmonic mechanical waves with amplitudes $\leq 1\mu m$. The information in the resulting displacement patterns is used to calculate characteristic properties of tissues, such as strain and other mechanical properties related to wave

propagation [19]. The mathematical basis of MRE will be derived here, following the treatment of Muthupillai et al. ([18],[19]).

In the presence of a magnetic-field gradient, the phase shift due to motion of spins is given by ([18],[19],[20]):

$$\phi(\tau) = \gamma \int_0^\tau \vec{G_r}(t) \cdot \vec{r}(t) dt, \tag{57}$$

where γ is the gyromagnetic ratio, $\vec{G_r}(t)$ is the time-dependent magnetic field gradient, $\vec{r}(t)$ is the position vector of the nuclei and τ is the gradient duration. In obtaining this result, rectangular gradients are assumed. Equivalently, equation (57) can be written as [18]:

$$\phi(\tau) = \gamma \int_0^\tau \left[\vec{G_r}(t) w(t)\right] \cdot \vec{r}(t) dt, \tag{58}$$

with:

$$w(t) = \begin{cases} 1 & \text{if } 0 < t < \tau \\ 0 & \text{Otherwise} \end{cases} \tag{59}$$

Equation (58) can be rewritten as [18]:

$$\phi(\tau) = \gamma \int_0^\tau \left[\int_{-\infty}^{\infty} \vec{\Gamma_r}(f) \exp(i2\pi f t) df w(t)\right] \cdot \vec{r}(t) dt, \tag{60}$$

where $\vec{\Gamma_r}(f)$ is the Fourier transform of $\vec{G_r}(t)$.
The equation above can be rewritten as [18]:

$$\phi(\tau) = \gamma \int_{-\infty}^{\infty} \vec{\Gamma_r}(f) \cdot \left[\int_0 \tau w(t) \vec{r}(t) \exp(i2\pi f t) dt\right] df, \tag{61}$$

which may be further simplified as[18]:

$$\begin{aligned} \phi(\tau) &= \gamma \int_{-\infty}^{\infty} \vec{\Gamma_r}(f) \cdot [F(w\vec{r})(-f)]\, df, & (62)\\ &= \gamma \int_{-\infty}^{\infty} \vec{\Gamma_r}(f) \cdot [F(w)(-f) * F(\vec{r})(-f)]\, df, & (63)\\ &= \gamma \int_{-\infty}^{\infty} \vec{\Gamma_r}(f) \cdot \left[W(-f) * \vec{R}(-f)\right] df, & (64) \end{aligned}$$

where $*$ represents the convolution operator, F represents the Fourier transform operator, and $W(f)$ and $\vec{R}(f)$ are the fourier transforms of $w(t)$ and $\vec{r}(t)$, respectively.
Equation (64) shows that the gradient function has a filtering property. As shown, the gradient function can be used as a basis function for estimating the harmonic displacement vectors of spins, as has been shown by Muthupillai et al. ([18],[19]). To estimate an arbitrary displacement vector, a set of three gradient functions, orthogonal over the integral duration, can be used as a basis [18].

Muthupillai et al. apply the theory derived above to the case of pure sinusoidal motion ([18],[19]):

$$\vec{r}(t) = \vec{r_0} + \vec{\xi_0} \exp(i(\vec{k} \cdot \vec{r} - \omega t + \alpha), \tag{65}$$

where $\vec{r_0}$ is the mean position of the nuclei, ξ_0 is the amplitude of displacement of the nuclei around their mean position, $\vec{k}$ is the wave number, α is the phase offset and ω is the angular frequency, which is equal to the frequency of the mechanical excitation.

The authors propose to consider the following gradient function ([18],[19]):

$$\left|\vec{G_r}(t)\right| = \begin{cases} +|G| & \text{if } t\epsilon \left[nT, (2n+1)\frac{T}{2}\right) \\ -|G| & \text{if } t\epsilon \left((2n+1)\frac{T}{2}, (n+1)T\right] \end{cases} \tag{66}$$

with $n = 0, 1, 2, ...N-1$, where N is the number of gradient cycles, and $T = \frac{2\pi}{\omega}$ and where $\tau = NT$ is chosen such that ([18],[19]):

$$\int_0^\tau \vec{G_r}(t) \cdot \vec{r}(t)dt = 0. \tag{67}$$

In this case, the phase shift is given by ([18],[19]):

$$\phi(\vec{r}, \alpha) = \frac{2\gamma NT(\vec{G_r} \cdot \vec{\xi_0})}{\pi} \sin(\vec{k} \cdot \vec{r} + \alpha). \tag{68}$$

As can be seen from equation (68), the phase shift is proportional to N, causing a high sensitivity to acoustic strain wave propagation, which is in general characterized by small amplitude cyclic displacement, as Muthupillai et al. discuss. Also, as we see from the equation above, the components of the motion along any desired axes can be estimated, as a consequence of the dot product which appears in the equation. Furthermore, the dependence of the phase shift upon the phase offset is apparent ([18],[19]).

The acquisition scheme used in MRE, a modified phase contrast gradient echo scheme with motion-sensitizing gradient waveforms in a balanced scheme, can be found in figure 2 [18]. With this scheme, acoustic strain waves (propagating shear waves) can be imaged. From the phase shift images, the displacement image can then be found by using equation (68), after accounting for the balanced acquisition scheme. The authors then use the displacement image to calculate the local wavelength in order to find a local shear modulus image, by using equation (50) ([18],[19]).

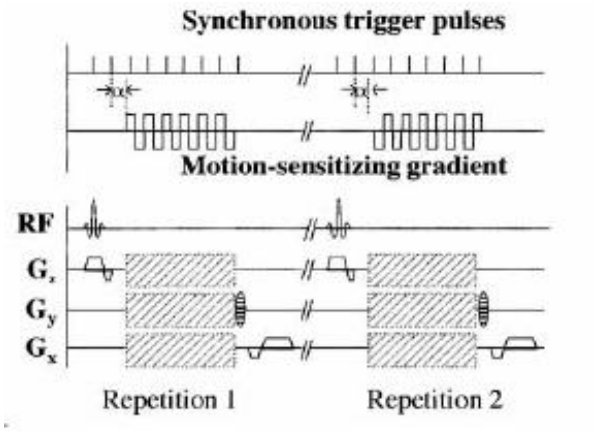

Figure 2: MRE sequence diagram. Trigger pulses for mechanical excitation produced by the MRI scanner are shown. The phase offset α between the trigger pulses and the motion-sensitizing gradient is variable. The shaded regions reflect the fact that the motion-sensitizing gradient waveforms can be applied along any arbitrary axis. Source: Muthupillai et al. [18]

The claims made above about the basis function property of the gradient waveforms have been checked by Muthupillai et al. [18] and found to be correct. Furthermore, refraction phenomena and dynamic wave propagation have been observed [18]. In the case of dynamic wave propagation, however, one needs to keep in mind that

a series of images are viewed which have been acquired by varying the phase offset, instead of a truly dynamic image.
To check the accuracy of the MRI displacement measurements, Muthupillai et al. use laser measurements as a gold standard. The measurements are shown to agree excellently, with $r^2 = 0.97$ [18] and in another independent measurement with $r^2 = 0.955$ [19].
Furthermore, Muthupillai et al. have performed measurements to show the feasibility of using their technique to quantitate the local shear modulus of material [19]. Comparison with static shear modulus measurements show the potential of the method to quantitatively measure the mechanical properties of tissue [19].

The authors compare their results to the results obtained with by Ophir et al. [1] and Plewes et al. [2]. As has been described in the previous section, Muthupillai et al. note that the need for boundary conditions and mathematical models in calculating the Young modulus is a difficulty arising in the methods developed by these authors ([18],[19]). However, Muthupillai et al. seem to overlook the fact that in obtaining shear modulus images, they themselves use mathematical models, which are a linear approximation.
Furthermore, concerning the method of Ophir et al. [1], Muthupillai et al. argue that the advantage of using MRI instead of using ultrasound is that with multiple acquisitions it is in principle feasible to calculate all components of the strain tensor. Also, volumetric acquisitions are feasible, at the penalty of acquisition times [18]. Moreover, the SNR and lateral resolution of MRE are claimed to be higher than those in ultrasound elastography [18].
Another advantage of MRE concerns the imaging of the shear modulus, as this modulus spans several orders of magnitude in tissues, unlike the bulk modulus. Thus, shear modulus imaging offers a better contrast mechanism in elasticity imaging.

Overall, the works of Muthupillai et al. ([18],[19]) show promising results for characterizing tissues by measuring their shear moduli. Both papers present a way to eliminate the use of boundary conditions in measuring displacement images ([1],[3],[2]). Furthermore, using the shear modulus to characterize tissues is useful for creating contrast [18], and may show promise as a potential technique for noninvasive 'palpation by imaging' ([18],[19]).

MRE has been compared to acoustic shear-wave imaging in a more elaborate way by Dutt et al. [22]. In their work they use the same theoretical basis for MRE as has been derived by Muthupillai et al. ([18],[19]) and which can be found above. Dutt et al. compare the displacement measured with MRE to the displacement measured with ultrasound.
To find the displacement with ultrasound measurements Dutt et al. integrate the doppler phase shift [23]:

$$\triangle\omega = \frac{2\frac{\partial\vec{\xi}}{\partial t}}{c} \cdot \vec{\omega}, \tag{69}$$

$$= 2\frac{\partial\vec{\xi}}{\partial t} \cdot \vec{k}, \tag{70}$$

which gives after integration:

$$\triangle\phi = 2\vec{\xi} \cdot \vec{k}, \tag{71}$$

where ω is the angular frequency, $\vec{\xi}$ represents the displacement of the tissue and $\vec{k}$ represents the wave-vector, which is parallel to the beam direction.
Using equation (71) Dutt et al. filter the ultrasound data to account for the intrinsic filtering of the MRE data by the alternating gradient waveform. The filtering is done at the material vibration frequency. The displacement parallel to the beam direction can now be found from the phase shift [22]:

$$D(\vec{r_0}, \tau) = \frac{1}{T}\int_{\tau-\frac{T}{2}}^{\tau+\frac{T}{2}} \triangle\phi(\vec{r_0}, \hat{\tau})\sin(\omega\hat{\tau})d\hat{\tau}. \tag{72}$$

From the experiments done Dutt et al. conclude that ultrasound imaging may be used as an alternative for MRE, even though MRE has a higher sensitivity and resolution, as can be seen from figure 6 in the paper of Dutt et al. [22]. The attractiveness of using ultrasound elastography is its cost-effectiveness, as the authors conclude [22]. However, as is apparent from the results obtained by Dutt et al. the MRE images look better deep into the phantom. And in addition, one must keep in mind the limitations of ultrasound imaging as discussed by Muthupillai et al. ([18],[19]), which have been described above. Thus, while ultrasound may be a cost-effective alternative in certain cases, one must not overlook the limitations of this technique, especially when imaging deep into tissue.

6.1.1 Applications

After having described the theory behind MRE and after having seen a comparison to US measurements, we will consider some applications.

Sinkus et al. describe the use of MRE to image breast lesions in vivo [24]. A novelty in their work is the use of the curl operator on the total displacement field obtained by MRE to ensure the removal of any contributions from the longitudinal wave.
Sinkus et al. use MRE to image breast lesions in vivo, analogously to the theory derived by Muthupillai et al. ([18],[19]). However, after obtaining the displacement images, the authors propose to apply the curl operator to the total displacement field. They argue that longitudinal and transverse waves are certainly not independent, while they interact via mode conversion at boundaries and interfaces, thus converting shear-waves into longitudinal (compressional) waves and vice versa [24]. Therefore, as the authors propose, the contributions originating from the longitudinal wave must be removed, as the other alternative of solely exciting shear-waves is almost infeasible [24].
After applying the curl operator, instead of using the linear shear-wave theory to calculate the shear modulus images, the authors consider nonlinear shear-wave propagation to be able to calculate the shear viscosity in addition to the shear modulus for every image [24].

As Sinkus et al. show there is a good correlation between their MRE findings and the anatomy. Furthermore, a good separation between benign and malignant lesions is found based upon the shear modulus. However, as the authors conclude from their results, the shear viscosity turns out to be less useful [24]. These results do not necessarily imply that the linear wave equation can be used, instead of the nonlinear wave equation to calculate the shear modulus, as the viscosity still influences the calculation of the shear modulus in the nonlinear shear wave equation. To say something about the accuracy of calculation of the shear modulus from the linear shear wave equation, it would be interesting to compare these results to the shear modulus as calculated from the nonlinear wave equation. However, this has not been done in literature yet.
Another interesting point would be to compare the results before application of the curl operator to the results after application of the curl operator. If application of the curl operator significantly improves the results and the additional time needed to apply the curl operator to the displacement images is small, the integration of this procedure into the standard MRE method can be considered.

The application of the curl operator to the displacement images described by Sinkus et al. [24], has also been used by Huwart et al. [25]. Here MRE is used for measuring liver stiffness in staging of liver fibrosis, where histology is used as a reference standard. In contrast to previously mentioned authors, Huwart et al. use the Voight model to calculate the shear elasticity maps, of which the mathematical theory can be found in Walker et al. [26].
In their study Huwart et al. compare a spin-echo sequence to a EPI sequence, where the rectangular displacement encoding gradients have been replaced by sinusoidal ones. The authors use respiratory gating in their study, while the liver is being imaged. Furthermore four temporal phases are recorded by changing the phase offset [25].
In their study Huwart et al. show that EPI is ten times as fast as spin-echo, while the SNR's are equal. Thus, as the authors conclude, EPI might well replace spin-echo in MRE, at least in measuring liver stiffness. However,

motion artifacts may appear more easily when using the EPI sequence [25].
Another thing one has to keep in mind, is that both Sinkus et al. and Huwart et al. use a relatively small test group in their studies ([24],[25]). Therefore, before drawing general conclusions larger studies need to be performed. However, in both cases the results regarding the application of MRE in clinical practise look promising ([24],[25]).

In a very recent paper by Siegmann et al. [27] the question of the diagnostic value of MRE in breast imaging is addressed. In this study the results of CE MRI are used to plan MRE, after identification of the target lesion on CE MRI. To allow a good comparison between the images, the patients are kept in the same position during the scans.
In their study Siegmann et al. use steady-state mechanical waves of 85 Hz as a compromise between low frequency waves, which show efficient wave penetration, and high frequency waves for sufficient spatial resolution.
Similar to the study done by Sinkus et al. [24], Siegmann et al. [27] use the non-linear shear wave equation to calculate the viscoelastic properties of the breast tissue. Again as shown by Sinkus et al., Siegmannn et al. show that the viscosity in combination with CE MRI is of little use. However, the authors convincingly show that a combination of CE MRI and the shear modulus leads to a higher specificity, by using ROC curves to support their claims, whereas both methods show worse results when used separately [27].
Even though, again, small test groups are used, the results imply that MRE may be used to improve the diagnosis of malignancy of breast lesions. Therefore this paper may well result in the use of MRE in clinic practise, if larger studies are done to support their findings [27].

All in all we may conclude that MRE is an upcoming technique that might provide additional diagnostic information in clinical practise [27]. More research still needs to be done to speed-up the procedures ([25]) and larger studies need to be performed to support the findings of the authors described above ([24],[25],[27]), but the method may provide insight in cases where the use of US elastography is limited. ([22])

6.2 Magnetic resonance elastography with focused ultrasound

Instead of using mechanical displacement to generate acoustic radiation force, as is done in the original MRE method as developed by Muthupillai et al. ([18],[19]), acoustic radiation force can also be generated by using focused ultrasound (FUS), as is described by Wu et al. [21].
Wu et al. use a single-element spherical shell air-backed FUS transducer to generate shear waves which are then imaged using the general MRE sequence displayed in figure 2 in order to generate displacement images. In stead of triggered mechanical pulses, Wu et al. propose to use 1.5 MHz focused ultrasound which is modulated by a rectangular envelope to create pulsed ultrasound. In this way Wu et al. induce shear waves in the focal region at the modulating envelope frequency [21].
Among the results obtained by Wu et al. graphs of the displacement at the FUS focal region in the longitudinal wave direction are displayed. From their results the authors conclude that this displacement is sinusoidal [21]. However, the authors do not use statistical tests to support their claims. For instance, it would be instructive to know if the fitting of two exponential functions gives better results, as is claimed by Huang et al. [28].
Wu et al. also compare the shear moduli calculated with their method to the shear modulus calculated from externally driven shear waves. The authors convincingly show that the results of these methods agree very well, with a correlation coefficient of 0.999 [21].
Furthermore, Wu et al. claim a linear relationship between FUS intensity and the displacement amplitude at the focus [21]. However, as we will see later in McDannold et al. [29], this claim is only true for low intensities. Also, a linear relationship between pulse duration and displacement at the focus is shown by Wu et al. [21]. However, intuitively, one could imagine that this is only true up to a certain point, where the counteracting elastic forces in the tissue balance the radiation force.
Although Wu et al. do not explicitly claim that these linear relationships are generally true, the authors could have been more careful to explicitly describe the range for which their results are valid.

Considering the results presented by Wu et al. and the discussion above about their validity, some parts of the conclusion from Wu et al. about their results leaves some unease. However,fortunately the fact that Wu et al. convincingly show that FUS may be used in MRE is not affected by their conclusions about linear or sinusoidal behavior.

Another interesting study concerning MRE with FUS has been done by Le et al. [30]. In their work the authors show that temperature can be measured simultaneous with MRE data. The authors propose to use two MRE measurements in order to be able to calculate both the phase difference due to motion and the phase difference due to the temperature difference. From these phase differences the displacement and the temperature difference can be calculated.
The results from the study of Le et al. indicate that MRE may be used for focused ultrasound therapy monitoring [30].

Even though there are still some issues to be cleared up in the study of Wu et al. [21], the outcomes do show that FUS may be used to generate shear waves. To accurately compare the results from MRE with FUS to the results from the original MRE method ([18],[19]), it would be instructive to calculate shear modulus images when using FUS. In this way a better comparison can be made with the results from Muthupillai et al. ([18],[19]) for example. However, with their work Wu et al. [21] do show the potential of using FUS in MRE measurements. Furthermore, the additional value of using FUS instead of mechanical excitation may be the possibility to simultaneously measure temperature differences [30].

7 Magnetic resonance acoustic radiation force imaging

While MRE uses shear waves to image elastic properties of tissues, another technique called MR-ARFI has been developed that measures the longitudinal displacement of tissue. However, this technique has not been used yet to image elastic properties of tissues, but only for imaging the displacement resulting from the application of focused ultrasound to the tissue.

MR-ARFI has been developed by McDannold and Maier [29]. McDannold and Maier use focused ultrasound instead of ordinary ultrasound to create larger displacements at deep tissue locations and to reduce the effect of tissue boundaries, such as mode conversion [29]. The authors choose to apply one long FUS pulse per acquisition and measures the displacement at the end of the FUS pulse. During the encoding gradients the tissue is presumed to be stationary instead of assuming cyclic motion by applying multiple pulses as in MRE ([18],[19]).
In their study which we will discuss later Huang et al. show that after 10 ms application of focused ultrasound, the motion has not reached steady state yet. However, it is difficult to compare their findings to the assumptions used by McDannold and Maier, as different experimental conditions are used.
McDannold and Maier use a one dimensional version of the method proposed by Plewes et al. [2]. A MR-ARFI sequence diagram can be found in figure 3.
McDannold and Maier propose to use a line sequence, of which the theoretical foundation can be found in Gudbjardsson et al. [31]. As explained by Gudbjardsson et al. the use of a line sequence reduces susceptibility and motion artifacts. Furthermore ghosting artifacts are completely absent as the method uses a single-shot ([29],[31]).
As can be seen from the MR-ARFI sequence diagram in figure 3, in the line sequence a $\frac{\pi}{2}$ RF pulse is followed by a π pulse to select two intersecting slices. While the FUS pulse is applied to the tissue, displacement encoding is done. After that a spin-echo is formed at the echo time from the column of intersection. During read-out, frequency encoding is done parallel to the FUS beam direction, which is along the column. This is repeated to obtain multiple columns in order to create a two dimensional image [29].
Two measurements are performed as described above, but with opposite gradient polarity. These two acquisitions are then subtracted to find a phase difference image, from which the displacement image can be found by

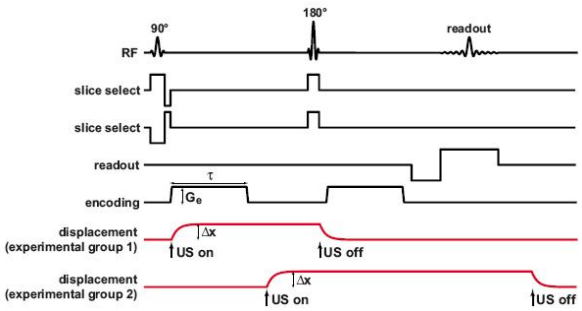

Figure 3: MR-ARFI sequence diagram. An MR-ARFI sequence diagram in combination with the assumed motion at the focus in the tissue. Two experiments are performed. The first group of experiments uses a 42 ms pulse. The second group uses a longer pulse of 75 ms. Source: McDannold and Maier [29]

using equation (56). Again, rectangular gradients are assumed to find this equation. However, as the authors note, the rise times of the trapezoidal gradients used are very small, the error is negligible.

With their measurements McDannold and Maier show that there is a linear relationship between acoustic power and displacement until $4W$. Above that power level, the linear relationship does not hold anymore. This is an addition to the results obtained by Wu et al. [21].
Also, for high acoustic power levels visible changes occur in the phantom. However, at the power levels used in their experiments, McDannold and Maier show that the temperature rise at the focus is smaller than 1^oC, thus ensuring that no visible changes will occur in the phantom [29].
Furthermore, as the authors observe, at high acoustic levels small transverse displacements are seen, orthogonal to the beam direction. Past the focal plane these displacements are directed away from the axis of beam propagation, while below the focal plane the displacements are directed towards the axis of beam propagation. It might be interesting to compare these results to the results obtained by Plewes et al. [2] as have been displayed in figure 4 in their work. In these images, the same pattern is found in the transverse x-direction as can be seen in the results obtained by McDannold et al. [29]. However, more research needs to be done in order to conclude if these results describe the same phenomenon.
McDannold and Maier also perform additional experiments on a bovine kidney in their study. They show that after ablation with focused ultrasound, the displacement at the focus increases by a small amount. The authors conclude that this may be used as a control mechanism in ablation therapy.

Improvement of the MR-ARFI method as developed by McDannold and Maier, has been proposed by Chen et al. [26]. In their work Chen et al. optimize the encoding gradients for MR-ARFI. They authors compare unipolar gradients (Stejskal Tanner gradients, as described by Haacke et al. [20]) which are generally used, to bipolar gradients, both repeated and inverted.
To improve the images acquired with unipolar gradients, the measurements need background phase correction, as has already been shown by McDannold and Maier [29]. The advantage of using bipolar gradients is that these do not require background phase correction, and in addition, they have enhanced SNR in the displacement map, which is contributed by the decreased diffusion-weighting of the bipolars [32]. Moreover, since repeated bipolars do not require background phase subtraction, SNR could be further improved by $\sqrt{2}$ [32].
With their study, Chen et al. show that the MR-ARFI is optimized by using repeated bipolars.

MR-ARFI has been compared to US-ARFI by Huang et al. [28].
Huang et al. claim that the motion of the tissue due to acoustic radiation force is near exponential both in the compression and in the relaxation phases, where $r^2 = 0.95$ and $r^2 = 0.93$ respectively. Their claim contradicts the findings of Wu et al. [21]. However, Wu et al. do not provide statistical information to support their claim,

so a comparison can not be easily made. Furthermore, based on their findings, Huang et al. question the validity of the sinusoidal model which has been used in MRE ([18],[19]).
Even though the motion is exponential, Huang et al. choose to use a quasi-static approach.
In order to make a better comparison between the MR-ARFI and the US-ARFI measurements, Huang et al. propose to use a two dimensional gradient echo with bipolar gradients for motion encoding, instead of using a line scan. However, as the authors discuss, the line scan is more efficient and appropriate for in vivo measurements, as is removes the need for multiple FUS pulses [28]. However, by using a line scan, the SNR is compromised [28].
The MR-ARFI sequence diagram used can be found in figure 4.

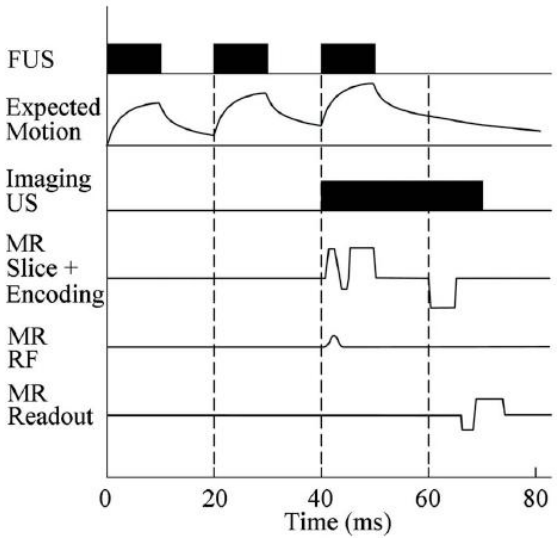

Figure 4: MR-ARFI sequence diagram as used by Huang et al. A two dimensional MR-ARFI sequence diagram in combination with the expected motion at the focus in the tissue. Source: Huang et al. [28]

Huang et al. use their results to claim that there is close agreement between the ultrasound and MR calculated displacement, with $r^2 = 0.67$ [28]. However, r^2 seems rather low here, in order to claim close agreement. As an explanation for the variability of the tissue displacement, the authors state that the tissue depth and tissue surrounding structures, such as bone, cause this variability. However, as one may expect that the same part of the tissue is imaged in order to compare the ultrasound and MR measurements, the presence of for example bony structures, should be visible in both measurements.
Furthermore, Huang et al. show that after 10 ms of pushing by the FUS beam at an acoustical power of 25 W, maximal displacement has not been obtained yet [28]. When we compare this to the results obtained by McDannold and Maier [29] it is difficult to check if maximal displacement has been reached in this case, as McDannold and Maier use a different FUS frequency, different FUS acoustical powers and different FUS pulse durations. However, as Huang et al. note, the use of a lower acoustic power with reduced displacement magnitude [29] and reduced time for tissue to reach a static displacement, may justify the assumptions made by McDannold and Maier.
One remarkable point apparent from the work of Huang et al. is the use of both MRE and MR-ARFI as a name for their method. The confusion is apparent, when realizing that MR-ARFI is originally a one dimensional method measuring longitudinal displacement, while MRE is originally a two dimensional method measuring shear displacement. However, Huang et al. use a two dimensional model to measure longitudinal displacement. The name giving in literature seems to be a bit arbitrary. If the MR-ARFI method would be extended to create elasticity images, the name MRE would apply equally well. Therefore a distinction between the methods based on the longitudinal or shear displacement imaging may be more appropriate.

MR-ARFI is still a relatively new MR method. Thus, not many applications can be found in literature yet, so little can be said about its effect in clinical practice. However, recently (June 2010) a study has been done about using MR-ARFI for US focusing in an application to US transcranial therapy.
Especially in transcranial therapy, FUS efficacy is degraded by aberrations caused by nonhomogeneous tissue which distort and shift the focus [10]. Hertzberg et al. propose to use MR-ARFI to measure the acoustic radiation force and to relate this to the phase of a group of elements of the FUS transducer [10].
The authors derive their theory by using the acoustic field of a phased array [10]:

$$\Phi(\vec{r}) = \sum_{i=1}^{n} \frac{a_i}{|\vec{r} - \vec{x_i}|} \exp\left(-i(\omega t + \phi_i)\right) \exp\left(ik|\vec{r} - \vec{x_i}|\right), \tag{73}$$

where n is the number of elements, $\vec{r}$ is the position in the field, $\vec{x_i}$ is the position of the ith element, k is the wave number and ω is the angular frequency.
Hertzberg et al. use the expression for the radiation force which can be found in equation (22) to find [10]:

$$|\vec{F}| = \frac{W}{c} = \frac{2\alpha}{c} I = \frac{2\alpha}{c} \left\langle \rho c (\nabla \Phi(\vec{r}))^2 \right\rangle_t \hat{n}, \tag{74}$$

where α is the absorption coefficient, c is the speed of sound and ρ is the medium density. The quantity I represents the acoustic intensity. A derivation of the second equality can be found in O'Brien [33].
Using far-field approximation Hertzberg use the equations above to show that [10]:

$$|\vec{F}| \propto \left(\cos(\tilde{\phi} - \tilde{\phi_j}) + \frac{\tilde{a^2} + \tilde{a_j^2}}{2\tilde{a} \cdot \tilde{a_j}} \right), \tag{75}$$

where $\tilde{a_i} = \frac{a_i}{|\vec{r} - \vec{x_i}|}$ and $\tilde{\phi_i} = \phi_i - k|\vec{r} - \vec{x_i}|$. Furthermore $\tilde{a} \exp(-i\tilde{\phi}) = \sum_{k \neq j}^{n} \tilde{a_k} \exp(-i\tilde{\phi_k})$ has been used.
Using equation (75) Hertzberg et al. show that modulating the phase of a single acoustic element ϕ_j results in modulation of the radiation force [10].
In their work Hertzberg et al. compare a line-scan spin-echo sequence to a gradient-echo EPI MR-ARFI sequence. The former sequence is the sequence developed by McDannold and Maier [29]. However, Hertzberg et al. choose to replace the unipolar displacement encoding gradients by inverted bipolar gradients, and give a reference to Chen et al. [32]. In choosing to replace the unipolars by inverted bipolars, the authors seem to have made a mistake, as Chen et al. show that repeated bipolars optimize the sequence as opposed to inverted bipolars [32].
In their experiment Hertzberg et al. split up the FUS transducer in four groups of elements and correct for the total phase of these elements, by using the displacement due to the radiation force at the focal point to correct for abberation [10]. In addition, the quality of the focus may be estimated by the displacement measurements, as the temperature rise which usually characterizes the focus quality, is proportional to the displacement [10].

In their comparison between the line-scan sequence and the EPI sequence, the authors show that the EPI sequence is advantageous over the line-scan sequence, due to its short acquisition time and low amount of energy per image [10]. The authors propose an improvement of their method by using multishot acquisitions with EPI sequences [10].
Furthermore, the results obtained by Hertzberg et al. show the potential of the method for focus localization. The abberation correction gives a near optimal focus, which is similar to the non-aberration case, as is shown by Hertzberg et al. [10]. This is an improvement of the usual method of aberration correction, using CT [10].
In addition, using an experiment where a pig brain is imaged through a human skull, the results obtained show that segment based adaptive focussing may be promising for human treatments, while the aberration correction provides a way to develop more reliable and safer brain FUS treatments [10].
Another difficulty in brain FUS treatments is the temperature increase, which must be kept smaller than 1^oC [11]. Fortunately, as the authors argue, this is the case [10].

Even though MR-ARFI is still a fairly new technique, and not many applications have been studied yet, its application for US focussing is clear from the study by Hertzberg et al. [10]. Also, as Hertzberg et al. note, its impact on US transcranial therapy may be large [10]. However, more research still needs to be performed in order to estimate the impact of this method on clinical practise.

8 Conclusions

Both MRE and MR-ARFI currently seem promising methods to be used in clinical practice, for instance in the diagnosis of liver fibrosis [25], in breast imaging ([24],[27]) and in ultrasound transcranial therapy [10]. In the latter MR-ARFI may be used to correct aberrations, in order to improve the focus of a FUS system, while in breast imaging, the use of MRE in addition to CE MRI leads to a higher specificity in lesion characterization. Furthermore MRE may be used to stage liver fibrosis noninvasively.
In order to integrate MRE and MR-ARFI into clinical practice, there are still some challenges to be faced. For example the imaging time needs to decrease, in order to increase patient comfort [27]. However, this may conflict with the wish to extend the methods to three dimensional routines, in order to integrate these methods into existing treatments. Furthermore, more research may be done regarding the risk of tissue ablation and cavitation during acoustic radiation force imaging, as little literature has been published yet considering these mechanisms.
As has been shown in multiple publications MR methods to image acoustic radiation force may be preferred to ultrasound methods in some cases ([22],[10],[28]), even though these MR methods are less cost-effective and not available in real-time yet. Moreover, MR methods, and especially MRE, have already proven to be quantitatively reliable and in good agreement with US measurements ([22],[28]. Therefore, MR methods to image acoustic radiation force may provide a good alternative for ultrasound methods when imaging deep in the body or in the brain, or when dealing with structures which are invisible to ultrasound.

Appendices

A Modified proof of Livett et al.

In their work Livett et al. [4] start with the general definitions of the Lagrangian and Eulerian coordinate systems:

$$p_L(x,t) = p_E(x+\xi,t), \tag{76}$$

where the subscripts L and E refer to the Lagrangian and Eulerian coordinate systems, respectively. Furthermore, x is the coordinate of a fluid element at time $t = 0$ and $\xi(x,t)$ is the displacement of that particle at time t [4].
The authors propose to use a Taylor expansion in equation (76):

$$p_L = p_E + \sum_{k=1}^{\infty} \frac{\xi^k}{k!} D^k[p_E] \equiv \exp^{\xi D}[p_E], \tag{77}$$

using $D^k[f]$ as a shorthand notation for the differential operation $\frac{\partial^k f}{\partial x^k}$, following the notation of Livett et al. [4].
The authors then write the one dimensional analogue of equation (8) as:

$$D[p_E] = -(\rho_E v_E)_t - D[\rho_E v_E^2], \tag{78}$$

where $()_t$ denotes differentiation with respect to time, using the notation of Livett et al. [4].
The authors substitute this expression into equation (77) and use the fact that $(\xi)_t \equiv u_L = \exp^{\xi D}[u_E]$ in combination with the identity $\exp^{\xi D}[u_E]\exp^{\xi D}[\rho_E u_E] = \exp^{\xi D}[\rho_E u_E^2]$ to obtain:

$$p_L = p_E + \rho_E u_E^2 - (\sum_{k=1}^{\infty} \frac{\xi^k}{k!} D\xi^{k-1}[\rho_E u_E])_t. \tag{79}$$

However, here Livett et al. [4]may have made a mistake.
To see this, we use the following expression, where partially integrating has been used:

$$\xi^k D^{k-1}(\rho_E u_E)_t = (\xi^k D^{k-1}[\rho_E u_E])_t - k\xi^{k-1}(\xi)_t D^{k-1}[\rho_E u_E]. \tag{80}$$

Using this expression, while substituting equation (78) into equation (77) gives:

$$p_L = p_E - \sum_{k=1}^{\infty}(\frac{\xi^k}{k!} D^{k-1}[\rho_E u_E])_t + (\xi)_t \sum_{k=1}^{\infty} \frac{\xi^{k-1}}{(k-1)!} D^{k-1}[\rho_E u_E] - \sum_{k=1}^{\infty} \frac{\xi^k}{k!} D^k[\rho_E u_E^2]. \tag{81}$$

Now using the previously mentioned identities $\exp^{\xi D}[u_E]\exp^{\xi D}[\rho_E u_E] = \exp^{\xi D}[\rho_E u_E^2]$ and $(\xi)_t \equiv u_L = \exp^{\xi D}[u_E]$, gives:

$$p_L = p_E + \rho_E u_E^2 - \sum_{k=1}^{\infty}(\frac{\xi^k}{k!} D^{k-1}[\rho_E u_E])_t + \exp^{\xi D}[u_E] \sum_{k=0}^{\infty} \frac{\xi^k}{(k)!} D^k[\rho_E u_E] - \exp^{\xi D}[u_E]\exp^{\xi D}[\rho_E u_E]. \tag{82}$$

The last step consists of recognizing that:

$$\exp^{\xi D}[\rho_E u_E] = \rho_E u_E + \sum_{k=1}^{\infty} \frac{\xi^k}{k!} D^k[\rho_E u_E], \tag{83}$$

so that:

$$p_L = p_E + \rho_E u_E^2 - (\sum_{k=1}^{\infty} \frac{\xi^k}{k!} D^{k-1}[\rho_E u_E])_t. \tag{84}$$

Now taking the time average of this equation, leads to the following identity:

$$\overline{p_L} = \overline{p_E} + \overline{\rho_E u_E^2}, \tag{85}$$

provided that we prove that the time average of the sum in equation (84) is equal to zero. Note that the right-hand side of the equation above is equal to the one dimensional radiation pressure.
To proof that the time average of the sum in equation (84) is equal to zero, we use equation (11):

$$\lim_{T\to\infty} \| \frac{1}{2T} \int_{-T}^{T} (\sum_{k=1}^{\infty} \frac{\xi^k}{k!} D^{k-1}[\rho_E u_E])_t dt \| \leq \lim_{T\to\infty} \| [\frac{\xi}{2T} \sum_{k=1}^{\infty} \frac{\xi^{k-1}}{(k-1)!} D^{k-1}[\rho_E u_E]]_{t=-T}^{t=T} \|. \tag{86}$$

Now on the right-hand side of this inequality we recognize the exponent:

$$\lim_{T\to\infty} \| \frac{1}{2T} \int_{-T}^{T} (\sum_{k=1}^{\infty} \frac{\xi^k}{k!} D^{k-1}[\rho_E u_E])_t dt \| \leq \lim_{T\to\infty} \| [\frac{\xi}{2T} \exp^{\xi D}[\rho_E u_E]]_{t=-T}^{t=T} \|. \tag{87}$$

While ρ_E and u_E are physical functions, both they themselves and their derivatives must be bounded for all times t. Thus, the argument of the exponent must be bounded for all times t. This means that the limit must be zero, thus finalizing the proof of equation (85).

References

[1] J. Ophir, I. Céspedes, H. Ponnekanti, Y. Yazdi, and X. Li. **Elastography: a quantitative method for imaging the elasticity of biological tissues**. *Ultrasonic Imaging*, 1991.

[2] D.B. Plewes, I. Betty, S.N. Urchuk, and I. Soutar. **Visualizing tissue compliance with MR imaging**. *J. Magn. Reson. Im.*, 1995.

[3] I. Céspedes, J. Ophir, H. Ponnekanti, and N. Maklad. **Elastography: elasticity imaging using ultrasound with application to muscle and breast in vivo**. *ULtrasonic Imaging*, 1993.

[4] A.J. Livett, E.W. Emery, and S. Leeman. **Acoustic radiation pressure**. *Journal of Sound and Vibration*, 1981.

[5] W.B. Joyce. Radiation force and the classical mechanics of photons and phonons. *Am. J. Phys.*, 1975.

[6] G.R. Torr. **The acoustic radiation force**. *Am. J. Phys.*, 1984.

[7] L.D. Landau and E.M. Liftshitz. *Fluid Mechanics, Volume 6 of Course of Theoretical Physics*. Pergamon Press, 2nd edition, 1974.

[8] R.T. Beyer. *Nonlinear Acoustics*. Naval Ship Systems Command, Washington, DC, 1974.

[9] A.Y. Iyo. Acoustic radiation force impulse imaging: a literature review. *J. Diagn. Med. Son.*, 2009.

[10] Y. Hertzberg, A. Volovick, Y. Zur, Y. Medan, S. Vitek, and G. Navon. **Ultrasound focusing using magnetic resonance acoustic radiation force imaging: Application to ultrasound transcranial therapy**. *Med. Phys.*, 2010.

[11] W.F. Walker. Internal deformation of a uniform elastic solid by acoustic radiation force. *J. Acoust. Soc. Am.*, 1999.

[12] A.P. Sarvazyan, O.V. Rudenko, S.D. Swanson, J.B. Fowlkes, and S.Y. Emelianov. Shear wave elasticity imaging: a new ultrasonic technology of medical diagnosis. *Ultr. Med. Biol.*, 1998.

[13] O.V. Rudenko, A.P. Sarvazyan, and S.Y. Emelianov. Acoustic radiation force and streaming induced by focused nonlinear ultrasound in a dissipative medium. *J. Acoust. Soc. Am.*, 1996.

[14] L. Ostrovsky, A. Sutin, Y. Il'inskii, O. Rudenko, and A. Sarvazyan. Radiation force and shear motions in inhomogeneous media. *J. Acoust. Soc. Am.*, 2007.

[15] L.A. Ostrovsky. Radiation force in nonlinear, focused beams (l). *J. Acoust. Soc. Am.*, 2008.

[16] L.D. Landau and E.M. Liftshitz. *Theory of Elasticity, Volume 7 of Course of Theoretical Physics*. Pergamon Press, 2nd (revised) edition, 1970.

[17] A.S. Saada. *Elasticity, Theory and Applications*. Pergamon Press, 1974.

[18] R. Muthupillai, P.J. Rossman, D.J. Lomas, J.F. Greenleaf, S.J. Riederer, and R.L. Ehman. **Magnetic resonance imaging of transverse acoustic strain waves**. *Magn. Reson. Med.*, 1996.

[19] R. Muthupillai, D.J. Lomas, P.J. Rossman, J.F. Greenleaf, A. Manduca, and R.L. Ehman. **Magnetic resonance elastography by direct visualization of propagating acoustic strain waves**. *Science*, 1995.

[20] E.M. Haacke, R.W. Brown, M.R. Thompson, and R. Venkatesan. *Magnetic Resonance Imaging, Physical Principles and Sequence Design*. John Wiley & Sons, 1999.

[21] T. Wu, J.P. Felmlee, J.F. Greenleaf, S.J. Riederer, and R.L. Ehman. **MR imaging of shear waves generated by focused ultrasound**. *Magn. Reson. Med.*, 2000.

[22] V. Dutt, R.R. Kinnick, R. Muthupillai, T.E. Oliphant, R.L. Ehman, and J.F. Greenleaf. **Acoustic shear-wave imaging using echo ultrasound compared to magnetic resonance elastography**. *Ultr. Med. Biol.*, 2000.

[23] J.L. Prince and J.M. Links. *Medical Imaging, signals and systems*. Pearson Prentice Hall, 2006.

[24] R. Sinkus, M. Tanter, T. Xydeas, S. Catheline, J. Bercoff, and M. Fink. **Viscoelastic shear properties of in vivo breast lesions measured by MR elastography**. *J. Magn. Reson. Im.*, 2005.

[25] L. Huwart, N. Salameh, L. ter Beek, E. Vicaut, F. Peeters, R. Sinkus, and B.E. Van Beers. Mr elastography of liver fibrosis: preliminary results comparing spin-echo and echo-planar imaging. *Eur. Radiol.*, 2008.

[26] W.F. Walker, F.J. Fernandez, and L.A. Negron. A method of imaging viscoelastic parameters with acoustic radiation force. *Phys. Med. Biol.*, 2000.

[27] **K.C. Siegman and T. Xydeas and R. Sinkus and B. Kraemer and U. Vogel and C.D. Claussen**. Diagnostic value of mr elastography in addition to contrast-enhanced mr imaging of the breast - initial clinical results. *Eur. Radiol.*, 2010.

[28] Y. Huang, L. Curiel, A. Kukic, D.B. Plewes, R. Chopra, and K. Hynynen. **MR acoustic radiation force imaging: In vivo comparison to ultrasound motion tracking**. *Med. Phys.*, 2009.

[29] N. McDannold and S.E. Maier. **Magnetic resonance acoustic radiation force imaging**. *Med. Phys.*, 2008.

[30] Y. Le, O. Rouviere, R. Ehman, and J.P. Felmlee. Simultaneous temperature and tissue stiffness detection by mr elastography. *Therapeutic ultrasound: 5th international symposium on therapeutic ultrasound*, 2006.

[31] H. Gudbjartsson, S.E. Maier, R.V. Mulkern, I.Á. Mórocz, S. Patz, and F.A. Jolesz. Line scan diffusion imaging. *Magn. Reson. Med.*, 1996.

[32] J. Chen, R. Watkins, and K.B. Pauly. **Optimization of encoding gradients for magnetic resonance acoustic radiation force imaging**. *AIP Conf. Proc.*, 2009.

[33] W.D. O'Brien Jr. Ultrasound-biophysics mechanisms. *Progress in Biophysics and Molecular Biology*, 2007.